

Single-cell transcriptomic analysis revealed the tumor-associated microenvironment of papillary thyroid carcinoma with metastasis

NI ZHANG^{1*}, QINGBIN LIU^{2*}, QIAN WANG^{3*}, XIULI LIU⁴, SUYA ZHANG³, XINCHEN TIAN²,
LONG LI³, SHUANGLONG WANG³, BIN LV³ and SHULONG JIANG^{1,2}

¹Cheeloo College of Medicine, Shandong University, Jinan, Shandong 250000, P.R. China; ²Clinical Medical Laboratory Center, Jining First People's Hospital, Shandong First Medical University, Jining, Shandong 272000, P.R. China;

³Department of Ultrasonic Medicine, Jining First People's Hospital, Shandong First Medical University, Jining, Shandong 272000, P.R. China; ⁴Department of Breast and Thyroid Surgery, Jining First People's Hospital, Shandong First Medical University, Jining, Shandong 272000, P.R. China

Received September 5, 2024; Accepted November 1, 2024

DOI: 10.3892/ol.2025.14876

Abstract. Papillary thyroid cancer (PTC) is frequently associated with inflammation and lymph node metastasis. Single-cell RNA sequencing (scRNA-seq) is a powerful tool to uncover rare cellular subpopulations and investigate the diverse functions inside tissue microenvironments. In the present study, scRNA-seq analysis was employed to analyze the differences in macrophages, dendritic cells (DCs) and T cells between a metastatic PTC (PTC-M) and its adjacent normal tissues, as well as a PTC tumor without metastasis. The findings revealed significant heterogeneity in immune cell populations in PTC-M, suggesting that immunosuppressive components contribute to the development and metastasis of PTC. The current study revealed that the presence of

alternatively activated M2 macrophages, conventional type 2 DCs (DC2s) and regulatory T cells (Tregs) was associated with increased lymph node metastasis and a more advanced stage of cancer. On the other hand, monocytes and B cells may have a beneficial effect in fighting against tumors. A group of tumor-associated DC2s expressing both *LAMP3* and *CCL22* were shown to have a variety of immune-related ligands. These cells have the ability to attract CD4+ T cells through communication between cells in the microenvironment. In this study, the immunological composition was examined at the level of individual cells and new prospective treatment approaches for PTC-M were identified. The results support the hypothesis that myeloid cells and Tregs significantly contribute to tumor progression and metastasis by shaping the tumor microenvironment.

Correspondence to: Professor Shulong Jiang, Clinical Medical Laboratory Center, Jining First People's Hospital, Shandong First Medical University, 6 Jiankang Road, Jining, Shandong 272000, P.R. China

E-mail: jnsljiang@163.com

Professor Bin Lv, Department of Ultrasonic Medicine, Jining First People's Hospital, Shandong First Medical University, 6 Jiankang Road, Jining, Shandong 272000, P.R. China

E-mail: lvbin005@126.com

*Contributed equally

Abbreviations: PTC, papillary thyroid cancer; LN, lymph node; scRNA-seq, single-cell RNA sequencing; DCs, dendritic cells; PTC-M, metastatic PTC; cDC2s, conventional-type 2 DCs; Tregs, regulatory T cells; TAMs, tumor-associated macrophages; TME, tumor microenvironment; NT, non-tumor; GO, Gene Ontology; KEGG, Kyoto Encyclopedia of Genes and Genomes; UMAP, Uniform Manifold Approximation and Projection

Key words: papillary thyroid cancer, single-cell RNA sequencing, dendritic cell, microenvironment

Introduction

Thyroid cancers (TCs) are the predominant malignant neoplasms in the endocrine system, originating from thyroid follicular or parafollicular epithelial cells. The global incidence of TCs has increased significantly in recent years, with projections indicating continued growth over the next two decades (1,2).

Advancements in ultrasound detection technologies have led to a rise in the diagnosis of thyroid malignancies, particularly papillary thyroid carcinomas (PTCs). PTCs are a type of differentiated thyroid carcinomas (DTCs), which account for >90% of all DTCs (3). While PTC progresses gradually and can be managed with surgical intervention and radioactive iodine ablation, certain individuals may exhibit numerous lymph node (LN) metastases at the time of PTC detection, resulting in an unfavorable prognosis, elevated recurrence rate and significant mortality risk (4,5). It remains largely elusive whether the cellular microenvironment of PTC differs from that of the adjacent tissue and the mechanism by which immune cells orchestrate PTC-LN metastasis.

Prior research utilizing RNA-sequencing (RNA-seq) and deconvolution algorithms have revealed numerous immune

cells that are associated with PTC. Specifically, advanced PTC exhibited a greater infiltration of immune cells in comparison to early PTC and normal tissues. Evidence increasingly suggests that tumor-associated macrophages (TAMs), dendritic cells (DCs), mast cells and regulatory T cells (Tregs) play key roles in PTC progression (6-10). While numerous simulated methods may measure the amount of immune cell infiltration from RNA-seq data sets, their overall evaluation may obscure important distinctions between different cell types. The advent of single-cell (sc)RNA-seq, however, has allowed for a more detailed analysis of immune-cell subpopulations and their interactions within the tumor microenvironment (TME), offering novel insights into the biology of PTC metastasis.

The objective of the present study was to investigate the immunological atlas of PTC by utilizing scRNA-seq of tumor tissues from two patients with PTC. These patients had varying degrees of LN metastases and adjacent normal tissue. The findings unveiled notable variations in cellular constituents and the immunological microenvironments of tumor tissues compared to non-tumor (NT) tissue.

The present study found that TAMs, or alternatively activated (M2) macrophages, conventional-type 2 DCs (cDC2s), Tregs, monocytes and B cells have various roles in tumor progression or metastasis. An analysis of crosstalk between different cell types was also conducted. The present study aimed to enhance the comprehension of the PTC immune cell atlas and its associations with tumorigenic growth. This research offers valuable insights into the immune dynamics of PTC and could inform future immunotherapeutic strategies.

Materials and methods

Clinical samples. In the present study, the specimens from two female patients with PTC who underwent surgery at Jining First People's Hospital (Jining, China) and whose diagnosis was confirmed by histology were included. A metastatic PTC (PTC-M) tumor and its adjacent NT tissues were collected from a 44-year-old patient in June 2022, whose PTC metastasized to LNs in the III/IV/V/VI area of the left neck and VI regions of the right neck. Another tumor sample was taken from a 64-year-old patient with PTC without any metastasis in the LNs in the bilateral cervical area in June 2022. Both patients carried a BRAF gene mutation (V600E) that was revealed by PCR sequencing (data not shown) (11). The study was approved by the Ethics Committee of Jining First People's Hospital (Jining, China). All procedures carried out in this study were in line with ethical standards of the Helsinki Declaration (revised in 2013) and written informed consent was obtained from all participants. Although patient samples were collected after ethical approval was granted, the analysis performed was retrospective in nature, as the samples were collected after diagnosis and did not involve patient follow-up.

Tissue dissociation and preparation. The fresh tissues were stored in sCellLive® Tissue Preservation Solution (Singleron Biotechnologies) on ice after surgical removal within 30 min. The specimens were washed with Hank's Balanced Salt Solution three times, minced into small pieces and then digested with 3 ml sCellLive® Tissue Dissociation Solution (Singleron Biotechnologies) using the PythoN® Tissue Dissociation

System (Singleron Biotechnologies) at 37°C for 15 min. The cell suspension was collected and filtered through a 40-micron sterile strainer. The mixture was then centrifuged at 300 x g and 4°C for 5 min, and following removal of the supernatant, the pellet was gently suspended with PBS. Finally, the samples were stained with 0.4% Trypan blue, mixed thoroughly at room temperature and immediately evaluated for cell viability under a microscope.

Reverse transcription (RT), amplification and library construction. Single-cell suspensions (2×10^5 cells/ml) in PBS were loaded onto a microwell chip using the Matrix® Single Cell Processing System (Singleron Biotechnologies). The scRNA-seq libraries were constructed according to the protocol of the GEXSCOPE® Single Cell RNA Library Kits (Singleron Biotechnologies) as previously described (12). Briefly, Barcoding Beads are collected from the microwell chip, followed by reverse transcription of the mRNA captured by the Barcoding Beads and to obtain cDNA, PCR amplification. The amplified cDNA was then fragmented and ligated with sequencing adapters. Individual libraries were diluted to 4 nM, pooled and sequenced on a Novaseq 6,000 (Illumina, Inc.) with 150 bp paired-end reads.

Analysis of raw read data. Raw reads from scRNA-seq were processed to generate gene expression matrixes using the CeleScope (<https://github.com/singleron-RD/CeleScope>) v1.9.0 pipeline. In brief, raw reads were first treated with CeleScope to remove low-quality reads with Cutadapt v1.17 (13) to trim poly-A tail and adapter sequences. The cell barcode and Unique Molecular Identifier (UMI) were extracted. Subsequently, STAR v2.6.1a (14) was used to map reads to the reference genome GRCh38 (Ensembl v92 annotation) (Index of/pub/release-92/fastq/homo_sapiens). The counts of UMI and genes in each cell were acquired with feature Counts v2.0.1 (15) software and used to generate expression matrix files for subsequent analysis.

Quality control, dimension reduction and clustering. Cells were filtered by gene counts <200 and the top 2% gene counts and the top 2% UMI counts. Cells with >30% mitochondrial content were removed. After filtering, 23,949 cells were retained for the downstream analyses, with on average 2,905 genes and 9,155 UMIs per cell. Functions from Seurat v3.1.2 (16) were used for dimension reduction and clustering. Subsequently, the NormalizeData and ScaleData functions were employed to normalize and scale all gene expression and the top 2000 variable genes were selected with the FindVariableFeatures function for principal component analysis. Using the top 20 principal components, cells were separated into multiple clusters with FindClusters. Cell clusters were visualized using t-Distributed Stochastic Neighbor Embedding (t-SNE) or Uniform Manifold Approximation and Projection (UMAP) with Seurat functions RunTSNE and RunUMAP.

Analysis of differentially expressed genes (DEGs). To identify DEGs, the Seurat FindMarkers function was used based on the Wilcoxon likelihood-ratio test with default parameters and the genes expressed in >10% of the cells in a cluster and

with an average log (fold change) value >0.25 were selected as DEGs. For the cell type annotation of each cluster, the expression of canonical markers found in the DEGs was combined with information from the literature and the expression of markers of each cell type was displayed using heatmaps/dot plots/violin plots that were generated with Seurat's DoHeatmap/DotPlot/Vlnplot function. Doublet cells were identified as expressing markers for different cell types and removed manually.

Cell type annotation. The cell type identity of each cluster was determined based on the expression of canonical markers found in the DEGs using the SynEcoSys[®] database (<https://singleron.bio>). Heatmaps/dot plots/violin plots displaying the expression of markers used to identify each cell type were generated by Seurat v3.1.2 DoHeatmap/DotPlot/Vlnplot.

Pathway enrichment analysis. To investigate the potential functions of DEGs, Gene Ontology (GO) and Kyoto Encyclopedia of Genes and Genomes (KEGG) were used with the 'clusterProfiler' R package v4.0.2 (17). Pathways with an adjusted $P < 0.05$ were considered as significantly enriched. GO gene sets, including molecular function, biological process and cellular component categories, were used as references.

For Gene Set Variation Analysis (GSVA) pathway enrichment analysis, the average gene expression of each cell type was used as input data using the GSVA package (18).

Trajectory analysis. The cell differentiation trajectory was reconstructed with Monocle2 (19). DEGs were used to sort cells in an order of spatial-temporal differentiation. The DDRTree function was used to perform FindVariableFeatures and dimension-reduction. Finally, the trajectory was visualized using the plot_cell_trajectory function. Next, CytoTRACE (v0.3.3) (20) (a computational method that predicts the differentiation state of cells from scRNA-seq data using gene counts and expression) was used to predict the differentiation potential of monocyte subpopulations.

Cell-cell interaction analysis. The cell-cell interaction analysis was performed using CellPhoneDB v2.1.7 (21) based on known receptor-ligand interactions between two cell types/subtypes. Cluster labels of all cells were randomly permuted 1,000 times to calculate the null distribution of average ligand-receptor expression levels of the interacting clusters. The individual ligand or receptor expression was thresholded with a cut-off value based on the average log gene expression distribution for all genes across all of the cell types. The significant cell-cell interactions were defined as having $P < 0.05$ and only receptors and ligands expressed in a threshold percentage of >0.1 of the cells in the specific cluster.

Multiplex immunohistochemistry (mIHC) assay and analysis. The Opal protocol staining approach was utilized to conduct mIHC staining, as previously described (22). mIHC was performed by several rounds of staining, each including a protein block with 1% BSA followed by addition of primary antibody and corresponding secondary horseradish peroxidase-conjugated antibody against mouse or rabbit immunoglobulins (ARH1001EA; Akoya

Biosciences). The slides were then incubated in different Opal fluorophores (1:100) diluted in 1X Plus Amplification Diluent (ARD1001EA; Akoya Biosciences). After tyramide signal amplification and covalent linkage of the individual Opal fluorophores (NEL861001KT; Akoya Biosciences) to the relevant epitope or epitopes, the primary and secondary antibodies were removed via antigen retrieval, as previously mentioned, and the next cycle of immunostaining was initiated. The primary antibodies and Opal fluorophores were as follows: Lysosomal associated membrane protein 3 (LAMP3; cat. no. ab134045; diluted 1:100; Abcam) was labeled using Akoya Opal fluorophores 520. C-C motif chemokine receptor 4 (CCR4; cat. no. NBPI-86584; diluted 1:100; Novus Biologicals) was labeled using Akoya Opal fluorophores 620. CD4 (cat. no. ab133616; diluted 1:100; Abcam) was labeled using Akoya Opal fluorophores 690. The nucleus was labeled with DAPI (diluted 1:100; Akoya). The cover-slipping of all sections was performed using Anti-Fade Fluorescence Mounting Medium (cat. no. ab104135; Abcam). Multichannel imaging was performed on a PANNORAMIC SCAN II Imaging System (3Dhistech Kft.). Image analysis was performed in QuPath V.0.5.1 (Queen's University) (23).

Results

A single-cell expression atlas of the PTC microenvironment. Single-cell RNA-seq analysis was performed on both metastatic tumor and adjacent NT tissues from a PTC case with aggressive metastasis (PTC-M). Additionally, the tumor tissue collected from a patient with non-metastatic PTC served as a control for comparison with the metastatic tumor. The clinical information of the patients was collected at the time of recruitment and was described in the methods section.

After stringent quality filtering, a total of 23,401 single cells were included in the analysis. Transcriptional data from all of the cells were integrated and low-resolution t-distributed stochastic neighbor embedding clustering was used to identify eight major cell populations. These populations were labeled as T cells (*CD3D*, *CD3E*, *CD2*, *TRAC*, *TRBC1* and *TRBC2*), B cells (*MS4A1*, *CD79A* and *CD79B*), plasma cells (*JCHAIN*, *MZB1* and *IGHG1*), mononuclear phagocytes (MPs) (*LYZ*, *CD14*, *CIQC*, *MRC1*, *CD68*, *CD163*, *CD1C* and *LAMP3*), endothelial cells (*PECAM1*, *VWF*, *CLDN5* and *CDH5*), mural cells (*ACTA2*, *TAGLN*, *MYLK*, *MYL9*, *PDGFRB* and *NOTCH3*), plasmacytoid dendritic cells (pDCs) (*IL3RA*, *CLEC4C*, *LILRB4* and *LILRA4*) and epithelial cells (*EPCAM*, *TG*, *DIO2*, *TACSTD2* and *KRT19*) (Fig. 1). A notable infiltration of MPs was observed in the PTC-M sample, where MPs accounted for 18.97% of total cells (998 cells), compared to only 1.92% in NT (148 cells) and 4.54% in PTC tissues (476 cells) (Fig. 1D). Fig. 1B displays the most distinct DEGs for each cell population.

Subtyping of MPs and their contributions to the immune microenvironment of PTC. MPs in PTC displayed increased expression of inflammation-related genes, including immune proteins (*LYZ*) and inflammatory cytokines (*CCL4*, *CCL3*, *CXCL8*, *CCL4L2* and *IL1B*), as well as human leukocyte antigens (HLA) (*HLA-DRA*, *HLA-DPA1* and *HLA-DRB1*) (Fig. 1B). DEG analysis revealed that the MPs in the PTC-M

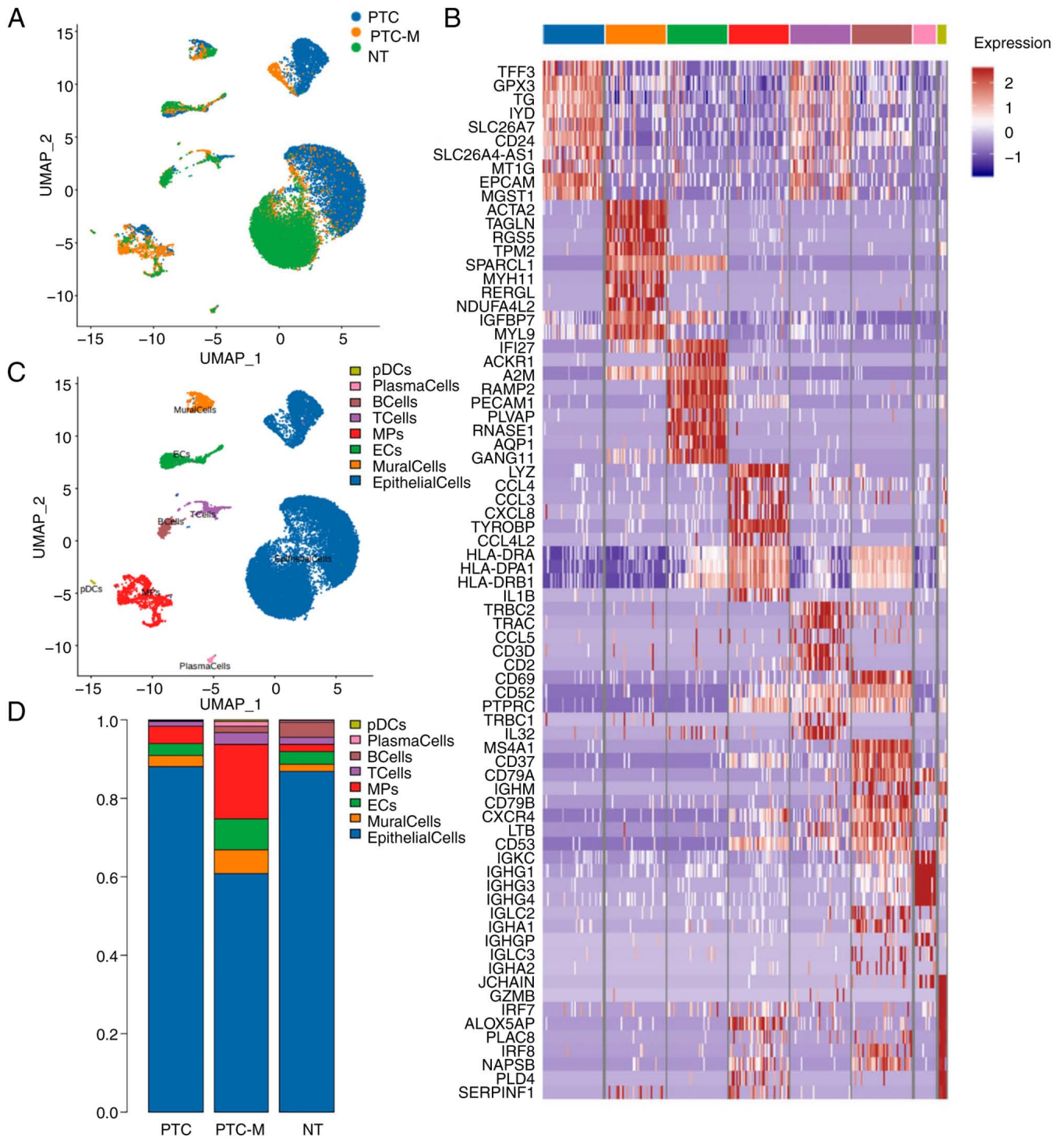


Figure 1. Transcriptome profiling of the PTC, PTC-M and NT tissues at the single-cell level. (A) UMAP plot visualization showed cell fractions in PTC, PTC-M and NT. (B) Heatmap of the top marker genes of cell lineages. (C) Cell populations are displayed with different colors. (D) The frequency of cell types in PTC, PTC-M and NT is shown in a bar graph. PTC-M, metastatic papillary thyroid cancer; NT, non-tumor; UMAP, Uniform Manifold Approximation and Projection; ECs, endothelial cells; pDCs, plasmacytoid dendritic cells; MPs, mononuclear phagocytes.

tumor tissue expressed a higher level of immune-suppression-related genes, such as *MRC1*, *CD163*, *CCL18*, *SPPI*, *CCL2*, *CCR2*, *CD40*, *CCL17* and *CCL22*, whereas exhibiting lower levels of *TNF*, *IL1B* and *RGS1* (Fig. S1A) when compared to the MPs from NT. The GO and KEGG analyses showed that the upregulated genes in MPs from PTC-M were mostly enriched in pathways related to the immune-inflammatory response, including 'neutrophil activation', 'neutrophil

degranulation', '*Staphylococcus aureus* infection' and 'tuberculosis' (Fig. S1B and C).

By conducting UMAP analysis, four distinct MP subgroups infiltrating the tumors were identified: Monocytes (*LYZ*, *CD14*, *FCN1*, *VCAN* and *FCGR3A*), macrophages (*LYZ*, *MRC1*, *CD68*, *CD163*, *CIQC*, *APOE* and *MARCO*), cDC2s (*CD1C*, *CD1E* and *FCER1A*) and mature DCs (*LYZ*, *LAMP3* and *CCR7*) (Fig. 2A). Further analysis demonstrated that

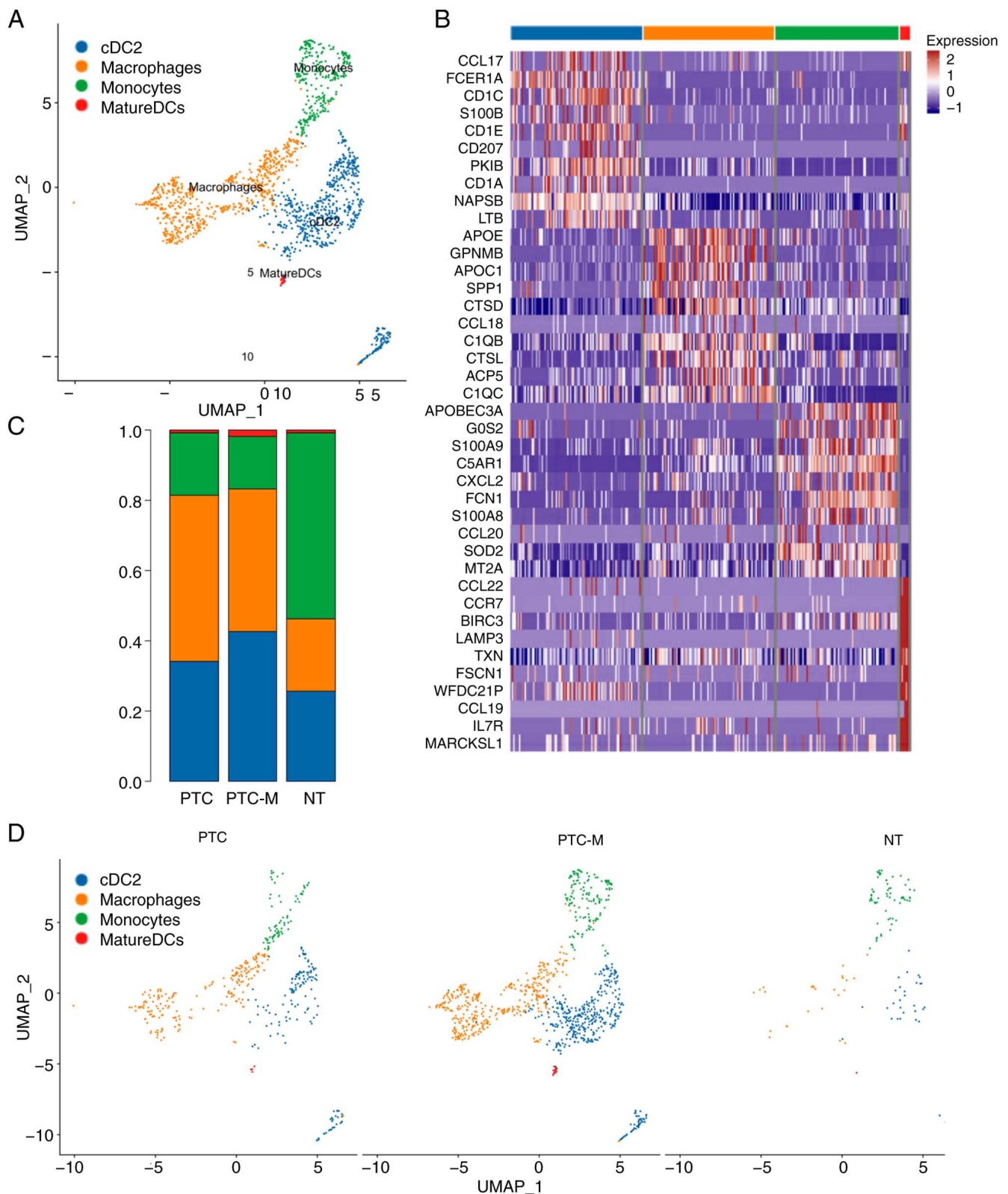


Figure 2. Identification and transcriptional characterization of MP subtypes. (A) UMAP projection of the four subtypes of MPs. (B) Heatmap of the top marker genes of monocytes, macrophages, cDC2 and mature DCs. (C) The composition of each MP subtype is displayed in a bar graph, with different colors representing the proportions of various MP subtypes in PTC, PTC-M and NT. (D) Different colors represent various MP subtypes, illustrating their composition in PTC, PTC-M and NT. cDC2s, conventional-type 2 dendritic cells; PTC-M, metastatic papillary thyroid cancer; NT, non-tumor; MP, mononuclear phagocyte; UMAP, Uniform Manifold Approximation and Projection.

cDC2s and macrophages made up 42.67 and 40.45% of MPs in the PTC-M sample, respectively. In the NT sample, monocytes were the most common MPs (52.89% of MPs; Fig. 2C and D).

Although a similar percentage of macrophage cells and cDC2s was found in PTC-M and PTC, the number of both subtypes of MP cell in PTC-M was ~2-fold higher than that in PTC

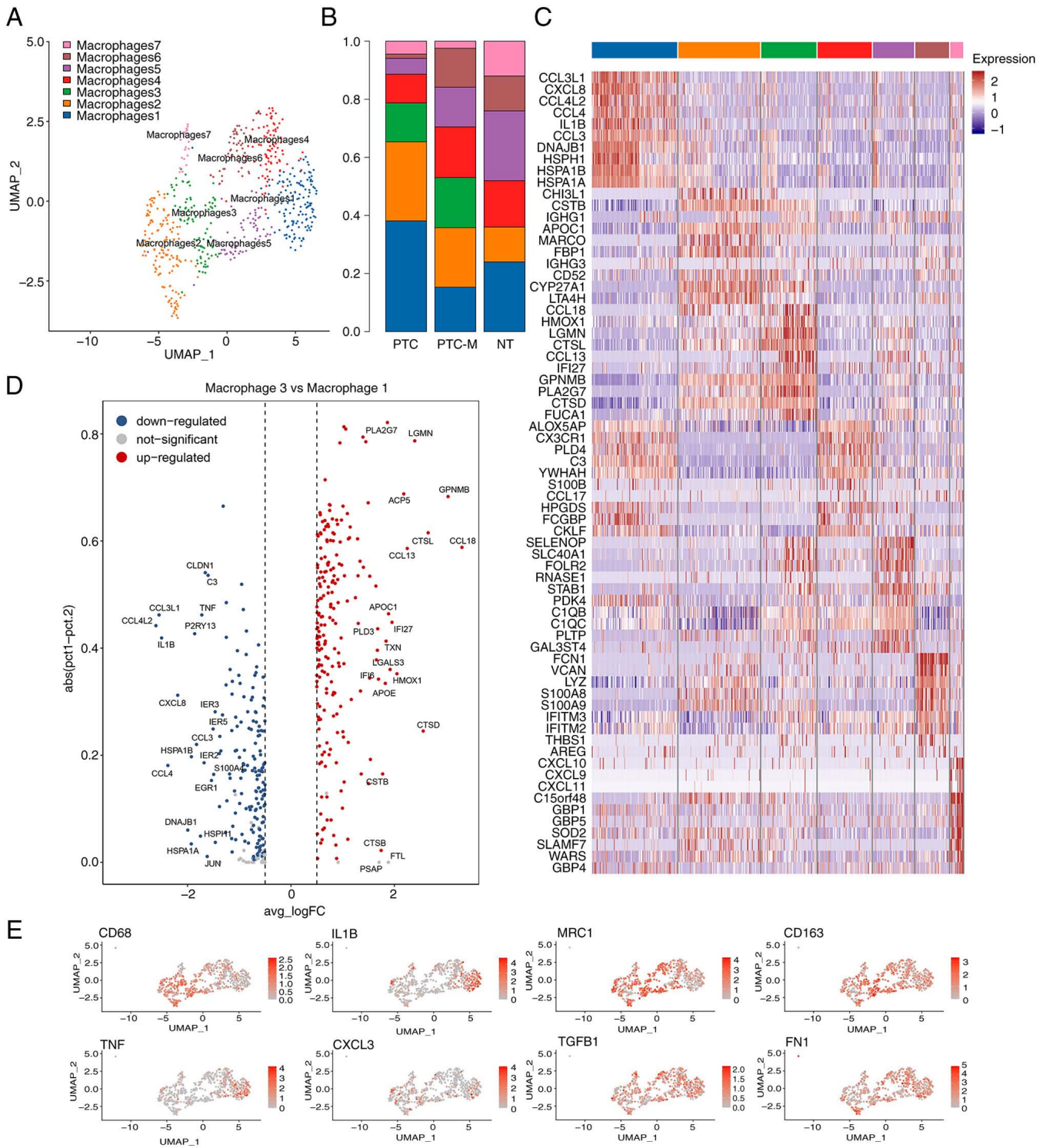


Figure 3. Characterization of M1- and M2-like macrophages. (A) UMAP projection of the different types of macrophages. (B) Percentages of macrophages in PTC, PTC-M and NT. (C) Heatmap of the top genes in each macrophage cluster. (D) Differential expression of genes between macrophage c3 and c1 clusters. (E) UMAP shows the distribution of key macrophage-associated genes for M1 and M2 clusters. UMAP, Uniform Manifold Approximation and Projection; PTC-M, metastatic papillary thyroid cancer; NT, non-tumor; FC, fold change; avg, average; abs, absolute.

(Fig. 2D). The top DEGs of each MP subtype are listed in Fig. 2B.

Immune-suppressive MRC1⁺CCL18⁺ M2 macrophages are enriched in PTC and PTC-M tissues. Macrophages were then annotated using UMAP and they were classified into 7 different clusters (Fig. 3A). Of note, the macrophage c3

cluster was solely enriched in PTC and PTC-M tumor tissues (Fig. 3A and B), demonstrating the unique tumor-associated function of immune-regulating macrophages. In addition, the macrophage c3 and c5 clusters expressed high levels of *MRC1*, *CD163* and *TGFBI* and low levels of *IL1B*, *TNF* and *RGS1*, which correspond to the alternatively-activated M2 subtype (Fig. 3C and D and Table SI) (24–26). It was

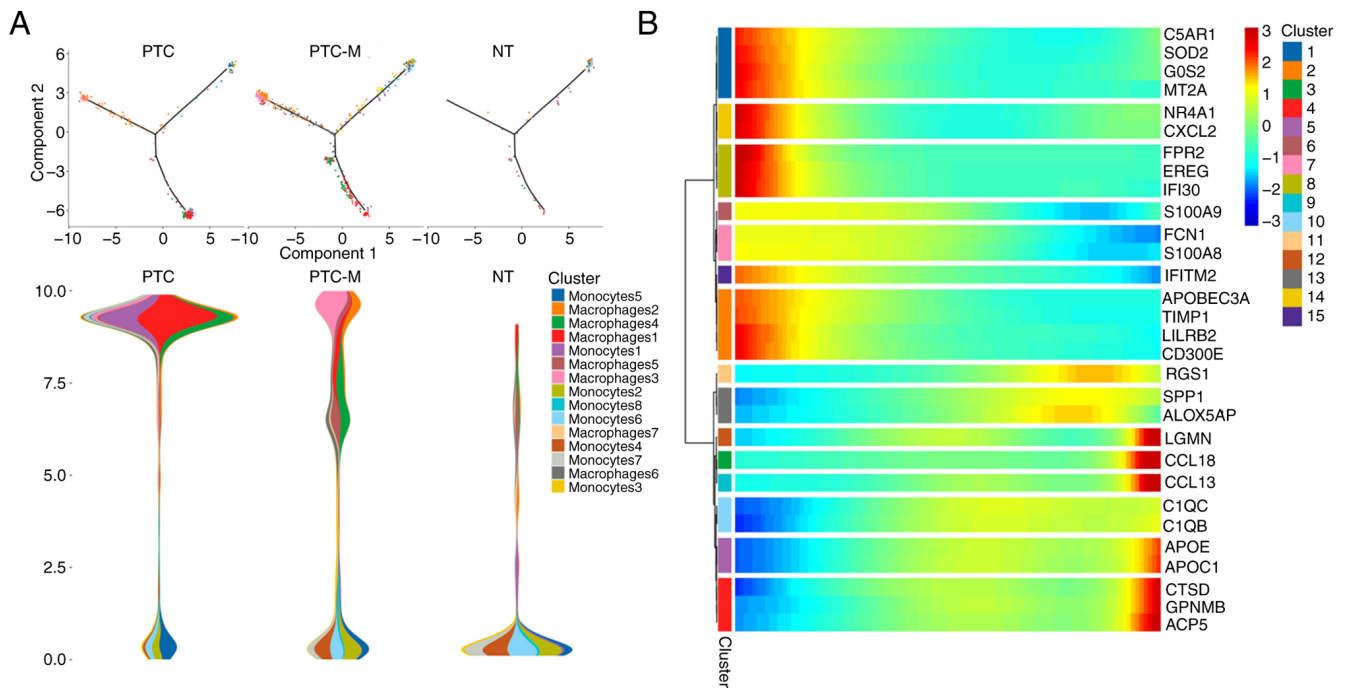


Figure 4. Progression and differentiation of monocyte-macrophage in PTCs. (A) Pseudotime plot and stream of monocyte-macrophage cells in PTCs revealed by Monocle2 analysis. (B) Heatmap showing the scaled expression of dynamic genes along the pseudotime. Rows of the heatmap represent the genes that show dynamic changes along the pseudotime. PTC-M, metastatic papillary thyroid cancer; NT, non-tumor.

also observed that *CCL18*, *SPP1*, *GPNMB*, *CCL2*, *CCL8* and *C1QA* were upregulated in the macrophage c3 cluster (*MRC1*⁺*CCL18*⁺ M2), while in the macrophage c5 cluster, the expression of *C1QB*, *C1QC* and *SLC40A1* was elevated (Fig. 3C; Table SI).

To analyze the TMEs potentially mediated by unique macrophage subtypes, DEG analysis was performed between the macrophage c1 and c3 clusters. Fig. 3D shows that in the macrophage c1 cluster, *IL1B*, *TNF* and *RGS1*, which are markers of classically-activated M1-type macrophages, were highly expressed (26), whereas the macrophage c3 subtype has a broad spectrum of molecules that are critical for pro-M2 conversions, such as *GPNMB*, or for inflammation, such as *CTSL*, *APOE* and *PLA2G7* (27-30). Furthermore, GO annotation analysis revealed 'positive regulation of cytokine production', 'leucocyte cell-cell adhesion' and 'T-cell activation' in c1 macrophages, while 'neutrophil activation' and 'neutrophil-mediated immunity' were more likely activated in c3 macrophages. In addition, KEGG enrichment analysis showed that c3 macrophage-expressed genes were enriched in the 'lysosome', 'phagosome', 'oxidative phosphorylation' and 'cholesterol metabolism pathways' (Fig. S2). Expression of classical macrophage M1 and M2 marker genes is shown in Fig. 3E. Since c1 was annotated as M1-like, while c3 and c5 were denoted as M2-like macrophages, the data revealed that the ratio of M2-like/M1-like macrophages substantially increased in the progressively advanced stage (38/77 in PTC vs. 113/56 in PTC-M) of PTC (Fig. 3B).

UMAP analysis was used to sub-classify the monocytes into 8 clusters. However, it was not possible to tell the difference between functional differences or differences in the make-up of groups in the PTC, PTC-M and NT samples. A cell trajectory analysis was then performed to further investigate the potential transition between

cell types. The pseudotime trajectory axis derived from Monocle indicates that monocytes could transdifferentiate into macrophage clusters, particularly c1 and c3 macrophages. The results illustrated that most monocytes remained quiescent in the NT sample, while they preferentially differentiated into the M1-like c1 macrophages in the PTC sample and more cells were directed towards the M2-like c3 macrophages in the PTC-M sample (Fig. 4A). Pseudotemporal expression patterns of representative genes also indicated the transition of monocytes into various macrophage clusters (Fig. 4B). These findings clearly outline the potential paths of differentiation for monocytes at a signal-cell level and suggest that they have the ability to give rise to a metastatic environment.

LAMP3⁺*CCL22*⁺ DCs with potential immune-suppressive capacity in PTC-M sample. DCs have a crucial function in presenting antigens, initiating T-cell responses and migrating to lymph nodes (31). By applying a UMAP analysis, 6 clusters of cDC2s were identified (Fig. 5A and C). The cDC2 c1 cluster was the predominant cluster in the NT tissue and exhibited significant expression of *IL1B*, *CCL3*, *CCL4*, *ATF3* and *CXCL8* (Fig. 5B). The cDC2 clusters c2, c4 and c6 showed significant enrichment in the PTC-M sample. The cDC2 c4 cluster was specifically studied because it shared similarities with the subtype of 'mature DCs enriched in immunoregulatory molecules' (mregDCs) that have the ability to migrate towards lymph nodes (32-34). The mregDCs-like cluster exhibited simultaneous expression of type 2 T-helper cell responsive genes (*CCL22* and *CCL17*) and other immune-regulatory genes (*C1QA* and *C1QC*), along with the DC maturation genes *LAMP3*, *CD40* and *CD80* (Fig. 5B; Table SII). By utilizing the feature plot and violin plot, it was possible to identify that the cDC2 c4 cells formed a distinct cluster characterized by elevated expression of immune-suppressive genes *LAMP3* and *CCL22*

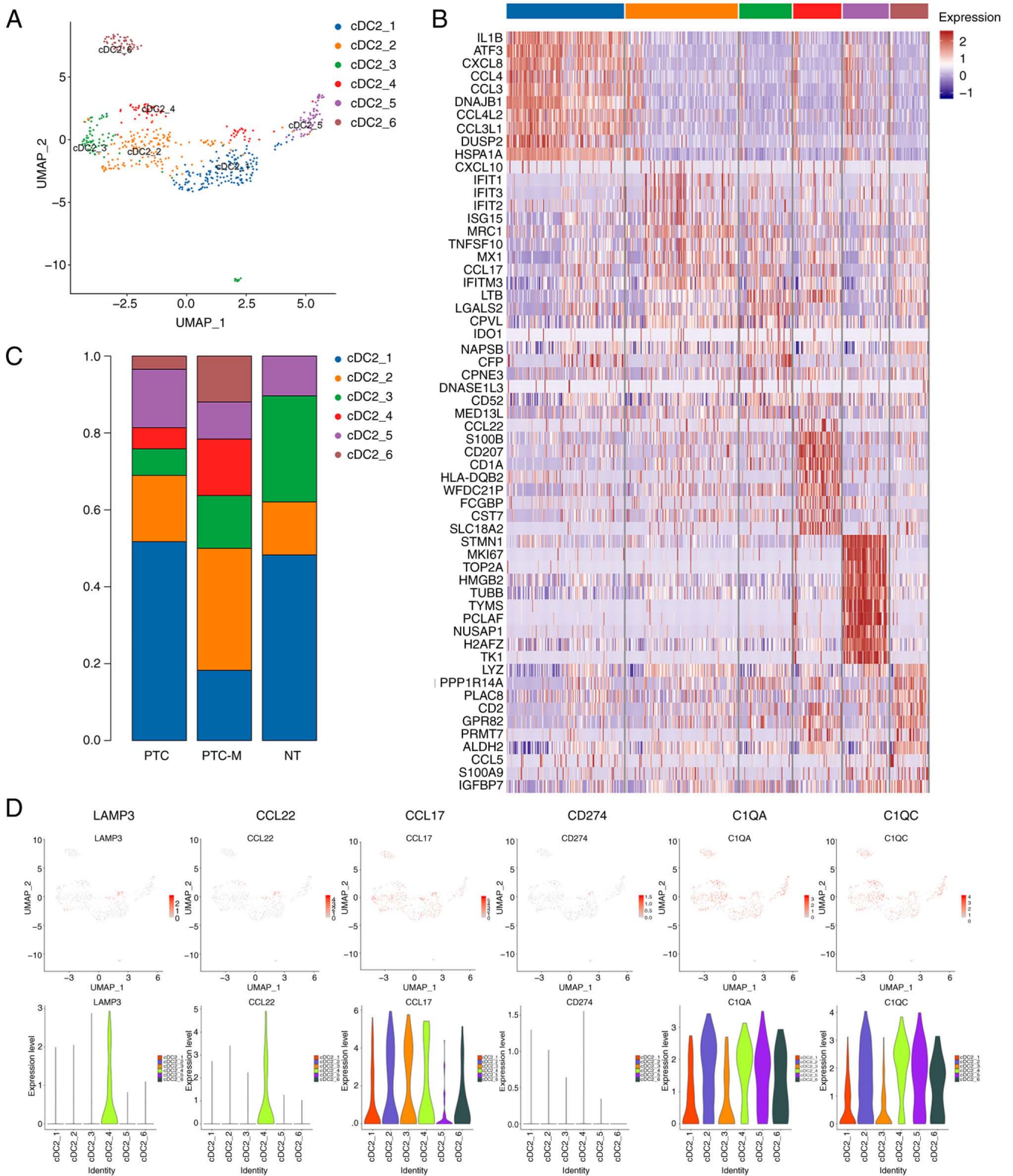


Figure 5. Molecular characteristics of subgroups of cDC2s. (A) UMAP projection of cDC2 clusters. (B) Heatmap of the top genes of each cDC2 cluster. (C) Percentage of each cDC2 cluster in PTC, PTC-M and NT sample. (D) Feature plot and violin plot display key mature and immune genes for cDC2 clusters. PTC-M, metastatic papillary thyroid cancer; NT, non-tumor; UMAP, Uniform Manifold Approximation and Projection; cDC2s, conventional-type 2 dendritic cells.

(*LAMP3*⁺*CCL22*⁺ DC) (Fig. 5D). Based on these observations, it may be proposed that the cDC2 c4 cluster likely functions as mregDCs, contributing to migration and the establishment of an immune-suppressive microenvironment in PTC-M.

Tumor-associated immune cell subtypes' crosstalk and their impact on the PTC microenvironment. To elucidate the interactions between different immune cell subtypes in the PTC microenvironment, a CellPhoneDB analysis was performed,

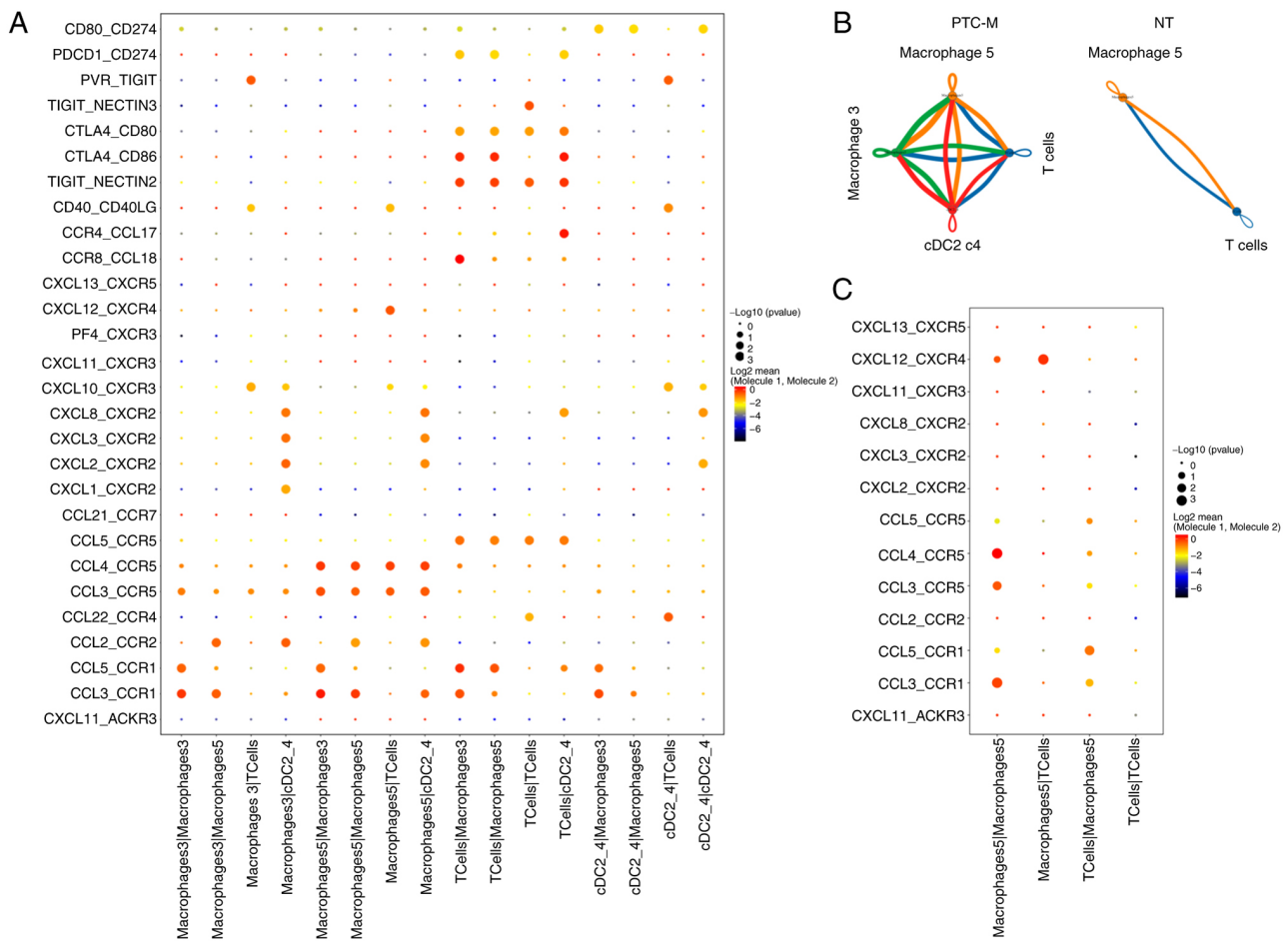


Figure 6. Contribution of macrophages and cDCs to the PTC microenvironment. (A) Bubble plots show ligand-receptor pairs of cytokines and chemokines between various cell types in PTC-M, inferred by CellPhoneDB. (B) Communications among major cell types in PTM-M and NT. (C) Ligand-receptor pairs of cytokines and chemokines between various cell types in NT tissue. PTC-M, metastatic papillary thyroid cancer; NT, non-tumor; cDC2s, conventional-type 2 dendritic cells.

focusing on ligand-receptor (L-R) interactions among macrophages, DCs and T cells (21). Based on the prior analysis, it was found that the majority of the projected crosstalk took place between macrophages c3, c5, cDCs c2 and T cells (Fig. 6A and B). Treg markers, such as TIGIT and CTLA-4, were expected to facilitate various immune-suppressive interactions between macrophages and DCs (35). In addition, it was projected that macrophage c3 and cDCs c2 could interact with Treg cells through the *CCL18-CCR8* complex and *CCL22-CCR4* complex, respectively (Fig. 6A) (36). The presence of cell-cell contacts was predominantly observed in the PTC-M sample, while being rare in the NT sample (Fig. 6B and C). It is worth mentioning that there are likely communications between cDCs c2 and macrophages in the tumor-associated environment and these communications are projected to be facilitated by the *CXCL2/3/8-CXCR2* complex (Fig. 6A; Table SIII). In summary, the present data showed that the cDCs c2 subtypes had the strongest association with CD4⁺ T cells in terms of L-R pair and were possibly linked to the infiltration or dysfunction of T-cell subtypes.

cDC2s associated with CD4⁺ T and Treg cell infiltration in the advanced stage of PTC. In order to comprehend the function of T cells in the microenvironment, UMAP was used

to categorize T cells into four distinct subclasses, including CD4⁺ naive T cells (*CD4*, *CCR7*, *LEF1*, *SELL*, *TCF7* and *IL7R*), Treg cells (*CD3D*, *FOXP3*, *IL2RA*, *CTLA4* and *IKZF2*), CD8⁺ effector T cells (*CD3D*, *CD8A/B*, *NKG7*, *GZMA* and *GNLY*) and proliferating T cells (*TOP2A*, *MKI67* and *CD3D*) (Fig. 7A and C). Unsurprisingly, PTC-M tissue exhibited over four times the amount of T-cell infiltration and a greater proportion of Tregs compared to NT and PTC tissues, indicating a more immune-suppressive milieu in PTC-M (Fig. 7C). Fig. 7B displays the manifestation of distinct T-cell marker genes. Based on the examination of cell-cell communication, it was observed that the majority of interactions took place between the cDC c2 cluster and T cells (Fig. 6B; Table SIII). Upon further examination, the application of mIHC staining on PTC-M tumor sections allowed for the clear observation of the close proximity of *LAMP3*⁺ mregDCs and *CCR4*⁺ T cells (Fig. 7D). The ligand-receptor pair showed a specific enrichment in the PTC-M tissue, indicating its connection with the development of tumors and the metastasis of cancer in this particular malignancy.

Discussion

Currently, there is a limited understanding of the specific immune cells involved in aggressive thyroid tumors. The

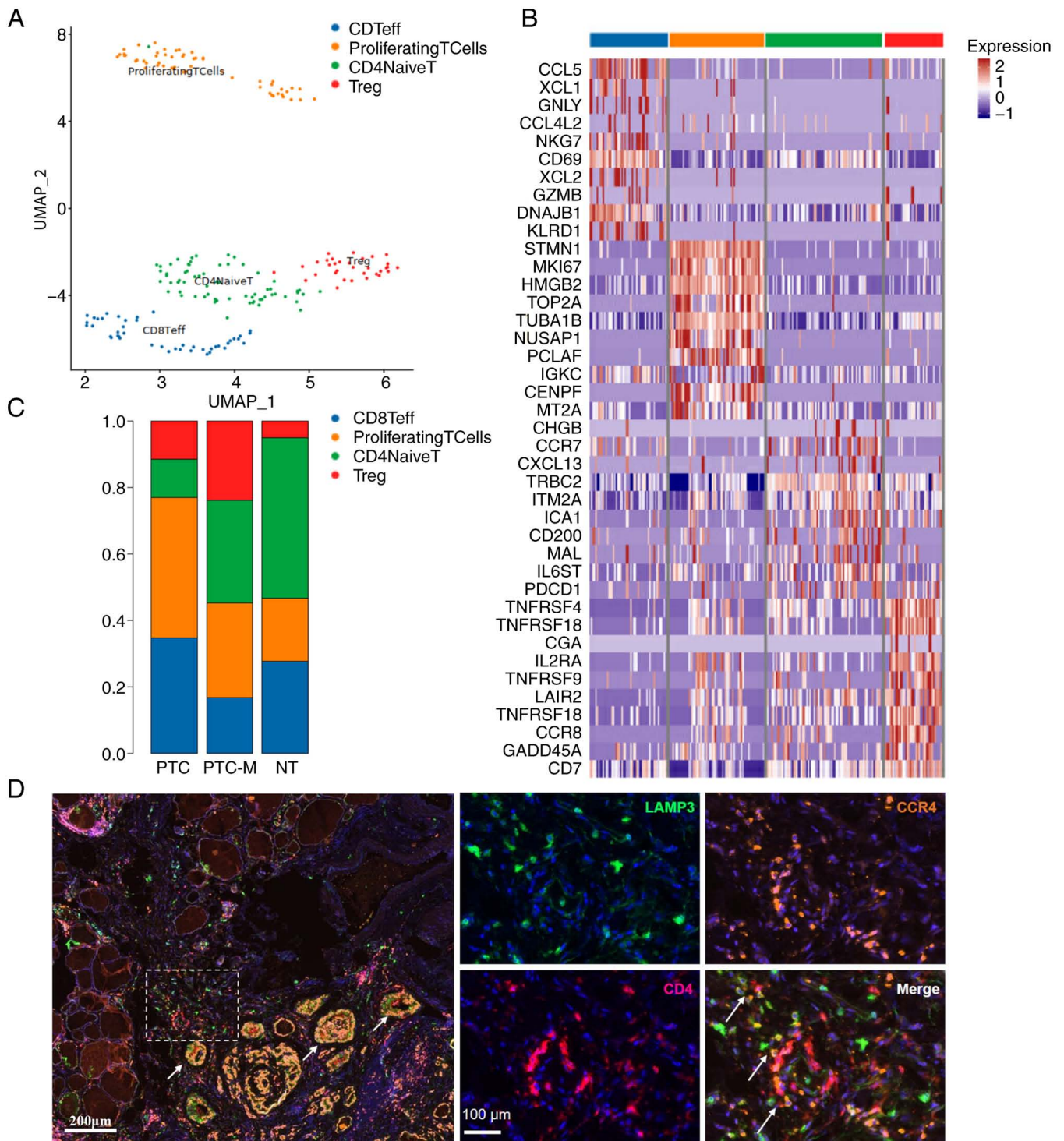


Figure 7. Characterization of Tregs and their crosstalk with mregDCs in PTC tissues. (A) UMAP projection of the different types of T cells. (B) Heatmap showing differential expression of genes in T-cell clusters. (C) Percentage of Teff cells, Treg cells, proliferating T cells and Naive T cells in PTC, PTC-M and NT tissues. (D) Representative image illustrating the interaction between mregDCs and Tregs in PTC-M tissue, which was immuno-stained by multicolor immunohistochemistry with antibodies against LAMP3 (green), CD4 (red) and CCR4 (purple). The scale bar in the larger figure to the left represents 200 μ m, with a magnification of x4. The scale bar in the right figure represents 100 μ m and white arrows indicate the colocalization. PTC-M, metastatic papillary thyroid cancer; NT, non-tumor; UMAP, Uniform Manifold Approximation and Projection; mregDCs, mature dendritic cells enriched in immunoregulatory molecules; Treg cell, T-regulatory cell; Teff cell, effector T cell.

present study focused on characterizing the immune micro-environment in PTCs. The results demonstrated that the PTC with metastases exhibited a higher degree of immune infiltration. Tumor-associated M2 macrophages, DCs and Treg cells collaborated to create a tumor-promoting environment

within the tumor tissue. In contrast, B cells, monocytes and M1 macrophages, which are typically beneficial in healthy tissues, are significantly reduced in PTC tumors. In the present investigation, a small population of NK cells and neutrophils was observed. However, it was not possible to

categorize them into distinct clusters and the knowledge of the role of NK cells and neutrophils in the immune milieu of PTC thus remains limited. Various computational methods have been used to analyze PTC data in the TCGA cohort. These methods indicate that the presence of immune cells that promote tumor growth was significantly higher throughout the occurrence and advancement of PTC (6,9,37). Furthermore, it was hypothesized that TAMs and DCs produced from PTCs could potentially play a role in the differentiation of Tregs and the subsequent suppression or evasion of the immune system (7,10,38). Our findings provide strong evidence that an inflammatory environment plays a critical role in PTC progression and is particularly prominent in advanced stages. The immuno-suppressive environment in PTC is predominantly regulated by mononuclear phagocytes, specifically macrophages and dendritic cells, based on the percentage of immune cells. In particular, a group of M2-like macrophages expressing *MRC1* and *CCL18* (*MRC1*⁺*CCL18*⁺ M2), as well as a group of cDC cells expressing *LAMP3* and *CCL22*, which have characteristics similar to mregDCs, were identified. Furthermore, there was a noticeable abundance of these two groups of cells in metastasis-associated immune infiltration, accompanied by a greater ratio of Treg cells in the aggressive PTC-M. These cells could exert a pivotal influence on the development of tumors and the metastasis of cancer cells, which warranted a thorough examination of their associations.

M2-like TAMs have been detected in cases of lung cancer, breast cancer and hepatocellular carcinomas (33,39-41). The metastatic lesion of colorectal cancer in the liver is characterized by the infiltration of immunosuppressive cells, specifically *SPPI*⁺ macrophages and *MRC1*⁺*CCL18*⁺ M2-like macrophages (25). In the present study, a similar TAM subtype was discovered in the PTC tumors that has both a high phagocytosis capability and a strong oxidative phosphorylation signature.

Recent studies have also identified distinct cDC clusters in hepatocellular carcinoma, lung cancer, neck squamous cell carcinoma (42) and non-malignant inflamed tissue (43). The mature cDCs expressing *LAMP3*, *CCL22* and *CCL19* found in hepatocellular carcinoma are capable of migrating from tumors to lymph nodes. Despite certain variations in the expression profiles, these cells exhibited similarities to a subtype of mature dendritic cells that are abundant in immunoregulatory molecules. They were classified as mregDCs.

Within the PTC-M sample, a robust infiltration of dendritic cells was detected that harbored a specific subtype of *LAMP3*⁺*CCL22*⁺*CCL17*⁺ mregDCs. The CellPhoneDB study showed that both *MRC1*⁺*CCL18*⁺ macrophages and *LAMP3*⁺*CCL22*⁺ mregDCs in the PTC-M tissue communicated with Tregs through several ligand-receptor complexes, particularly *CCL22*-*CCR4* and *CCL18*-*CCR8*. Through the utilization of mIHC, it was possible to observe the contact between *LAMP3*⁺*CCL22*⁺ mregDCs and Tregs. The mregDC cluster cells are expected to interact with Tregs through the ligand-receptor pairs *CCL22*-*CCR4* and *CCL17*-*CCR4*, which then leads to the activation of Tregs and their infiltration into the tumor microenvironment. This observation indicates that immunotherapy targeting cytokines/chemokines could be a promising method for treating advanced PTC (44,45). In addition, CellPhoneDB predicted interactions between *LAMP3*⁺*CCL22*⁺ cDCs and *MRC1*⁺*CCL18*⁺ macrophages

through CXCR2-CXCL2/3/8 complexes, highlighting the need for further research to elucidate the regulatory mechanisms between these myeloid cells.

One limitation of the present study is the relatively small sample size, which may impact the generalizability of the present findings. While the single-cell RNA sequencing data provide valuable insight into the immune landscape of PTC, the limited number of samples reduces the statistical power and may not fully capture the heterogeneity of the immune microenvironment, particularly across different patient populations. In addition, our findings lack functional experimental validation, which is necessary to confirm the specific roles of immune cell subtypes, such as M2 macrophages and mregDCs, in tumor progression. Future studies with larger cohorts and functional assays are essential to validate these observations and further explore the underlying mechanisms in PTC.

To summarize, the present single-cell analysis of immune cells in metastatic and non-metastatic PTC provides evidence of the presence and makeup of immune cells in PTCs at a single-cellular level. Our research reveals distinct lineages and aggressive associations among macrophages, cDCs and Tregs clusters in advanced PTC. These findings offer vital knowledge and tools for further exploration of metastatic PTC and may guide the development of new treatment options for advanced PTC.

Acknowledgements

Not applicable.

Funding

This study was supported by grants from the Doctoral Fund of Jining First People's Hospital (grant no. 2020005), Jining Key Research and Development Program (grant nos. 2022YXNS133, 2023YXNS075 and 2023YXNS223), Shandong Medical and Health Science and Technology Development Plan Project (grant no. 202101040510), the National Natural Science Foundation of China (grant nos. 82074360), the Natural Science Foundation of Shandong Province (grant no. ZR2022LZY027) and the Young Taishan Scholars Program of Shandong Province (grant no. tsqn201909200).

Availability of data and materials

All data are available in the main manuscript or supplemental data. The raw sequencing data reported in this paper have been deposited in the Genome Sequence Archive (Genomics, Proteomics & Bioinformatics 2021) at the National Genomics Data Center (Nucleic Acids Res 2022), China National Center for Bioinformation/Beijing Institute of Genomics, Chinese Academy of Sciences (PRJCA027425). These data are publicly accessible at <https://ngdc.cnbc.ac.cn/gsa-human/browse/HRA007797>.

Author's contributions

Conceptualization was performed by SJ and BL. Data was analyzed by NZ, SZ, QW, XT, LL and QL. SZ, QW, SW and

QL performed the experiments. Original draft preparation was by NZ, SZ, QW and QL. Sample collection was performed by XL. Manuscript reviewing and editing was performed by LL, SW and QL. LL, XT and QL visualized the study. SJ supervised the study, and SJ and QL acquired funding. QL and SJ confirm the authenticity of all the raw data. All authors have read and approved the final version of the manuscript.

Ethics approval and consent to participate

This work was reviewed and approved by the Ethics Committee of Jining First People's Hospital (Jining, China; approval no. 2021-038). The patients/participants provided their written informed consent to participate in this study in June 2022. The study was performed in accordance with the Declaration of Helsinki.

Patient consent for publication.

Written consent was obtained from the participants to publish their patient data.

Competing interests

The authors declare that they have no competing interests.

References

- Pizzato M, Li M, Vignat J, Laversanne M, Singh D, La Vecchia C and Vaccarella S: The epidemiological landscape of thyroid cancer worldwide: GLOBOCAN estimates for incidence and mortality rates in 2020. *Lancet Diabetes Endocrinol* 10: 264-272, 2022.
- Cheng F, Xiao J, Shao C, Huang F, Wang L, Ju Y and Jia H: Burden of Thyroid Cancer From 1990 to 2019 and Projections of Incidence and Mortality Until 2039 in China: Findings From Global Burden of Disease Study. *Front Endocrinol (Lausanne)* 12: 738213, 2021.
- Cabanillas ME, McFadden DG and Durante C: Thyroid cancer. *Lancet* 388: 2783-2795, 2016.
- Suh YJ, Kwon H, Kim SJ, Choi JY, Lee KE, Park YJ, Park DJ and Youn YK: Factors affecting the locoregional recurrence of conventional papillary thyroid carcinoma after surgery: A Retrospective Analysis of 3381 Patients. *Ann Surg Oncol* 22: 3543-3549, 2015.
- Zhan L, Feng HF, Yu XZ, Li LR, Song JL, Tu Y, Yuan JP, Chen C and Sun SR: Clinical and prognosis value of the number of metastatic lymph nodes in patients with papillary thyroid carcinoma. *BMC Surg* 22: 235, 2022.
- Pu W, Shi X, Yu P, Zhang M, Liu Z, Tan L, Han P, Wang Y, Ji D, Gan H, *et al*: Single-cell transcriptomic analysis of the tumor ecosystems underlying initiation and progression of papillary thyroid carcinoma. *Nat Commun* 12: 6058, 2021.
- Xie Z, Li X, He Y, Wu S, Wang S, Sun J, He Y, Lun Y and Zhang J: Immune cell confrontation in the papillary thyroid carcinoma microenvironment. *Front Endocrinol (Lausanne)* 11: 570604, 2020.
- Galdiero MR, Varricchi G and Marone G: The immune network in thyroid cancer. *Oncoimmunology* 5: e1168556, 2016.
- Yan T, Qiu W, Weng H, Fan Y, Zhou G and Yang Z: Single-Cell transcriptomic analysis of ecosystems in papillary thyroid carcinoma progression. *Front Endocrinol (Lausanne)* 12: 729565, 2021.
- Bergdorf K, Ferguson DC, Mehrad M, Ely K, Stricker T and Weiss VL: Papillary thyroid carcinoma behavior: Clues in the tumor microenvironment. *Endocr Relat Cancer* 26: 601-614, 2019.
- Bentz BG, Miller BT, Holden JA, Rowe LR and Bentz JS: B-RAF V600E mutational analysis of fine needle aspirates correlates with diagnosis of thyroid nodules. *Otolaryngol Head Neck Surg* 140: 709-714, 2009.
- Dura B, Choi JY, Zhang K, Damsky W, Thakral D, Bosenberg M, Craft J and Fan R: scFTD-seq: Freeze-thaw lysis based, portable approach toward highly distributed single-cell 3' mRNA profiling. *Nucleic Acids Res* 47: e16, 2019.
- Martin M: Cutadapt removes adapter sequences from high-throughput sequencing reads. *EMBnet J* 17: 10-12, 2011.
- Dobin A, Davis CA, Schlesinger F, Drenkow J, Zaleski C, Jha S, Batut P, Chaisson M and Gingeras TR: STAR: Ultrafast universal RNA-seq aligner. *Bioinformatics* 29: 15-21, 2013.
- Liao Y, Smyth GK and Shi W: featureCounts: An efficient general purpose program for assigning sequence reads to genomic features. *Bioinformatics* 30: 923-930, 2014.
- Satija R, Farrell JA, Gennert D, Schier AF and Regev A: Spatial reconstruction of single-cell gene expression data. *Nat Biotechnol* 33: 495-502, 2015.
- Yu G, Wang LG, Han Y and He QY: clusterProfiler: An R package for comparing biological themes among gene clusters. *OMICS* 16: 284-287, 2012.
- Hänzelmann S, Castelo R and Guinney J: GSVA: Gene set variation analysis for microarray and RNA-seq data. *BMC Bioinformatics* 14: 7, 2013.
- Qiu X, Hill A, Packer J, Lin D, Ma YA and Trapnell C: Single-cell mRNA quantification and differential analysis with Census. *Nat Methods* 14: 309-315, 2017.
- Gulati GS, Sikandar SS, Wesche DJ, Manjunath A, Bharadwaj A, Berger MJ, Ilagan F, Kuo AH, Hsieh RW, Cai S, *et al*: Single-cell transcriptional diversity is a hallmark of developmental potential. *Science* 367: 405-411, 2020.
- Efremova M, Vento-Tormo R, Teichmann SA and Vento-Tormo R: CellPhoneDB: Inferring cell-cell communication from combined expression of multi-subunit ligand-receptor complexes. *Nat Protoc* 15: 1484-1506, 2020.
- Carstens JL, Correa de Sampaio P, Yang D, Barua S, Wang H, Rao A, Allison JP, LeBleu VS and Kalluri R: Spatial computation of intratumoral T cells correlates with survival of patients with pancreatic cancer. *Nat Commun* 8: 15095, 2017.
- Bankhead P, Loughrey MB, Fernández JA, Dombrowski Y, McArt DG, Dunne PD, McQuaid S, Gray RT, Murray LJ, Coleman HG, *et al*: QuPath: Open source software for digital pathology image analysis. *Sci Rep* 7: 16878, 2017.
- Skytte MK, Graversen JH and Moestrup SK: Targeting of CD163+ Macrophages in Inflammatory and Malignant Diseases. *Int J Mol Sci* 21: 5497, 2020.
- Wu Y, Yang S, Ma J, Chen Z, Song G, Rao D, Cheng Y, Huang S, Liu Y, Jiang S, *et al*: Spatiotemporal immune landscape of colorectal cancer liver metastasis at single-cell level. *Cancer Discov* 12: 134-153, 2022.
- Huang X, Li Y, Fu M and Xin HB: Polarizing macrophages in vitro. *Methods Mol Biol* 1784: 119-126, 2018.
- Lv SL, Zeng ZF, Gan WQ, Wang WQ, Li TG, Hou YF, Yan Z, Zhang RX and Yang M: Lp-PLA2 inhibition prevents Ang II-induced cardiac inflammation and fibrosis by blocking macrophage NLRP3 inflammasome activation. *Acta Pharmacol Sin* 42: 2016-2032, 2021.
- Tang TT, Lv LL, Pan MM, Wen Y, Wang B, Li ZL, Wu M, Wang FM, Crowley SD and Liu BC: Hydroxychloroquine attenuates renal ischemia/reperfusion injury by inhibiting cathepsin mediated NLRP3 inflammasome activation. *Cell Death Dis* 9: 351, 2018.
- Rebeck GW: The role of APOE on lipid homeostasis and inflammation in normal brains. *J Lipid Res* 58: 1493-1499, 2017.
- Zhou L, Zhuo H, Ouyang H, Liu Y, Yuan F, Sun L, Liu F and Liu H: Glycoprotein non-metastatic melanoma protein b (Gpmb) is highly expressed in macrophages of acute injured kidney and promotes M2 macrophages polarization. *Cell Immunol* 316: 53-60, 2017.
- Guilliams M, Ginhoux F, Jakubzick C, Naik SH, Onai N, Schraml BU, Segura E, Tussiwand R and Yona S: Dendritic cells, monocytes and macrophages: A unified nomenclature based on ontogeny. *Nat Rev Immunol* 14: 571-578, 2014.
- Maier B, Leader AM, Chen ST, Tung N, Chang C, LeBerichel J, Chudnovskiy A, Maskey S, Walker L, Finnigan JP, *et al*: A conserved dendritic-cell regulatory program limits antitumour immunity. *Nature* 580: 257-262, 2020.
- Zhang Q, He Y, Luo N, Patel SJ, Han Y, Gao R, Modak M, Carotta S, Haslinger C, Kind D, *et al*: Landscape and dynamics of single immune cells in hepatocellular carcinoma. *Cell* 179: 829-845.e20, 2019.

34. Liu W, Hu H, Shao Z, Lv X, Zhang Z, Deng X, Song Q, Han Y, Guo T, Xiong L, *et al*: Characterizing the tumor microenvironment at the single-cell level reveals a novel immune evasion mechanism in osteosarcoma. *Bone Res* 11: 4, 2023.
35. Rowshanravan B, Halliday N and Sansom DM: CTLA-4: A moving target in immunotherapy. *Blood* 131: 58-67, 2018.
36. Rapp M, Wintergerst MWM, Kunz WG, Vetter VK, Knott MML, Lisowski D, Haubner S, Moder S, Thaler R, Eiber S, *et al*: CCL22 controls immunity by promoting regulatory T cell communication with dendritic cells in lymph nodes. *J Exp Med* 216: 1170-1181, 2019.
37. Yin H, Tang Y, Guo Y and Wen S: Immune microenvironment of thyroid cancer. *J Cancer* 11: 4884-4896, 2020.
38. Yu H, Huang X, Liu X, Jin H, Zhang G, Zhang Q and Yu J: Regulatory T cells and plasmacytoid dendritic cells contribute to the immune escape of papillary thyroid cancer coexisting with multinodular non-toxic goiter. *Endocrine* 44: 172-181, 2013.
39. He D, Wang D, Lu P, Yang N, Xue Z, Zhu X, Zhang P and Fan G: Single-cell RNA sequencing reveals heterogeneous tumor and immune cell populations in early-stage lung adenocarcinomas harboring EGFR mutations. *Oncogene* 40: 355-368, 2021.
40. Choi J, Gyamfi J, Jang H and Koo JS: The role of tumor-associated macrophage in breast cancer biology. *Histol Histopathol* 33: 133-145, 2018.
41. Chung W, Eum HH, Lee HO, Lee KM, Lee HB, Kim KT, Ryu HS, Kim S, Lee JE, Park YH, *et al*: Single-cell RNA-seq enables comprehensive tumour and immune cell profiling in primary breast cancer. *Nat Commun* 8: 15081, 2017.
42. Fan C, Wu J, Shen Y, Hu H, Wang Q, Mao Y, Ye B and Xiang M: Hypoxia promotes the tolerogenic phenotype of plasmacytoid dendritic cells in head and neck squamous cell carcinoma. *Cancer Med* 11: 922-930, 2022.
43. Zhang QY, Ye XP, Zhou Z, Zhu CF, Li R, Fang Y, Zhang RJ, Li L, Liu W, Wang Z, *et al*: Lymphocyte infiltration and thyrocyte destruction are driven by stromal and immune cell components in Hashimoto's thyroiditis. *Nat Commun* 13: 775, 2022.
44. Propper DJ and Balkwill FR: Harnessing cytokines and chemokines for cancer therapy. *Nat Rev Clin Oncol* 19: 237-253, 2022.
45. Berlatto C, Khan MN, Schioppa T, Thompson R, Maniati E, Montfort A, Jangani M, Canosa M, Kulbe H, Hagemann UB, *et al*: A CCR4 antagonist reverses the tumor-promoting microenvironment of renal cancer. *J Clin Invest* 127: 801-813, 2017.



Copyright © 2025 Zhang et al. This work is licensed under a Creative Commons Attribution-NonCommercial-NoDerivatives 4.0 International (CC BY-NC-ND 4.0) License.